FORUM GEOGRAFI
ISSN: 0852-0682 | E-ISSN: 2460-3945

HTTPS://JOURNALS.UMS.AC.ID/INDEX.PHP/FG/

*Original research article*

# 3D Map Application on Cave Geosites in Relationship to Cave Morphometry and Surface Geomorphology in Karst Areas at Ngalau Basurek Cave, Silokek Geopark

**Dipo Caesario[1,*], Bigharta Bekti Susetyo[1], Weni Kurnia Sari[2], Wahyu Budhi Khorniawan[3], Ridwan Ridwan[4]**

[1] Department of Geography, Faculty of Social Science, Universitas Negeri Padang, 25171, Indonesia
[2] Department of Electronics Engineering, Faculty of Engineering, Universitas Negeri Padang, 25171, Indonesia
[3] Department of Geological Engineering, Faculty of Engineering, Diponegoro University, 50275, Indonesia
[4] Ranah Minang Silokek Geopark Management Agency, Sijunjung Regency, 27554, Indonesia

[*)] Correspondence: caesariodipo@fis.unp.ac.id

**Citation:**
Caesario, D., Susetyo, B. B., Sari, W. K., Khorniawan, W. B., & Ridwan, R. (2024). 3D Map Application on Cave Geosites in Relationship to Cave Morphometry and Surface Geomorphology in Karst Areas at Ngalau Basurek Cave, Silokek Geopark. Forum Geografi. 38(2), 231-243.

**Article history:**
Received: 11 May 2024
Revised: 13 July 2024
Accepted: 26 July 2024
Published: 27 August 2024



## Abstract

On 2 January 2018, the local government proposed Silokek, a region in the Sijunjung Regency, West Sumatra Province, Indonesia, as a geopark, based on district rule number 188.45/3/KPTS-BPT-2018. This arrangement was based on the idea that a geopark would provide tourist destinations with natural tourism and archaeological, environmental, historical, educational, and cultural components in addition to geology, making this place an indirect example of a complex tourist destination. The Ngalau Basurek Cave is a geosite in this area that is a well-liked tourist destination, although it does not yet have a useful and instructive cave morphometry map. Producing cave morphometric data using the compass and step mapping method and geomorphological analyses of Landsat 8 image data is suggested to identify patterns of relationships with surface karst morphological features. A northeast dip angle trend was visible in the fresh limestone of the Kuantan Formation, which formed cave features as a result of dissolution. The dolinas, uvalas, and cone–kart features, which are represented on topographic maps (DEM-SRTM), demonstrate comparable trends. Dip-angle and strike-line trends were used to obtain a complete relationship between cave morphometry and surface geomorphology in Silokek Geopark.

Keywords: Cave Morphometry; Geomorphology; Karts; Kuantan Formation; Silokek Geopark.

## 1. Introduction

Over the course of the past twenty years, the rise of geotourism, fuelled by a growing demand for unique geological experiences, has resulted in the promotion of geological heritage and geodiversity across a wide range of global regions (Štrba & Molokáč, 2022). Geoparks are interconnected sites that set regulations for long-term preservation, enjoy geological treasures, and encourage the economic expansion of local people also (Frey, 2021; Justice, 2018). Geoparks are groups of sites with distinctive scientific significance, attraction, or rarity that form part of geological heritage. In addition to the geological aspect, geoparks should have connections to the environment, history, culture, and archaeology (Patzak & Eder, 1998). In addition, geoparks need to incorporate the concepts of conservation, education, and community empowerment to enhance the economic prospects and advantages of neighbouring communities (Ngwira, 2019).

In another region, the establishment of geoparks was motivated by the desire to safeguard global cultural heritage by expanding tourist interest in geosites representing cultural heritage, while geoheritage was poorly exposed (Sen *et al.,* 2023). While consistent with the global principles of sustainable tourism, the goals and objectives of establishing a geopark demand the ongoing enhancement and completion of geo-education, geo-conservation, and the creation of local economic value through tourism, which can become significant indicators for the development of sustainable geotourism and geoconservation (Antić *et al.,* 2022). Then, the ideas of "integrity of place" and "geology-based" criteria for assessment, in addition to concepts like "geotourism" that highlight geology, geomorphology, and geodiversity, are important for the environment and human activity (Kirchner & Kubalíková, 2014; Kubalíková, 2013). Therefore, a geosite should have scientific value, especially the geology at a geological heritage site, which can explain geological features and processes while understanding its unique significance from both aesthetic and scientific aspects (Afrasiabian *et al.,* 2021).

The convergence of increasing cave tourism potential, particularly in nations with abundant caves but hindered by economic and political instability, alongside the looming threat of geohazards in vulnerable localities, such as valleys and escarpment sites during rainy periods, underscores the critical need for proactive management strategies (Chiarini, 2022). Furthermore, evaluating geosites offers valuable insights into key areas for improvement, ranging from enhancing safety measures in geo-hazard-prone regions to leveraging the cultural and ecological significance of

geological sites for sustainable tourism development (Hassi, 2022). This synthesis emphasises the interconnected dynamics of economic opportunities, environmental risks, and strategic planning in the context of surveying and mapping urban geomorphology, geotourism, and geological conservation. This approach aims to enhance the fundamental understanding of the evolution of forms caused by both natural processes and human activities (Marjanović, 2021; Pica *et al.,* 2024).

## 2. Geology Regional of Silokek Geopark

One of Indonesia's current geoparks is the Silokek Geopark. On 30 November 2018, the Geopark received the status of a National Geopark (Kusuma, 2019). The Silokek Geopark is located in the Sijunjung Regency in West Sumatra. On top of that, this site has a variety of fascinating geological meanings in addition to its acknowledged historical significance. According to the regional geological map (Silitonga & Kastowo, 1995) and the geological interpretation map results of remote sensing imagery (Bahri & Suwijanto, 2014), three formations exist in the research area, three of which are Permian Carbon of the Kuantan Fm. (PCkl) and Batholiths of Granite (g1 and g2), both of which act as the basement of the pre-Tertiary Ombilin Basin, where the Ombilin Formation (Tmol and Tmou) is deposited, as illustrated in Figure 1. The lithology is composed of Pre-Cenozoic bedrock consisting of limestone from the Kuantan Formation of Carboniferous age (Husein *et al.,* 2018; Koesoemadinata, 1981) that create morphological characteristics of 10 km hills that span from northwest to southeast to construct this geosite, with one of which is the "Ngalau Basurek" Cave located. Karst limestone often forms the region's undulating plains (Fadhly & Hadiyansyah, 2020). The “Ngalau Basurek” (The Written Cave) Geosite may be found in West Sumatra's Muaro Sijunjung, Sijunjung District, and Sijunjung Regency, which can be classified in this criteria.

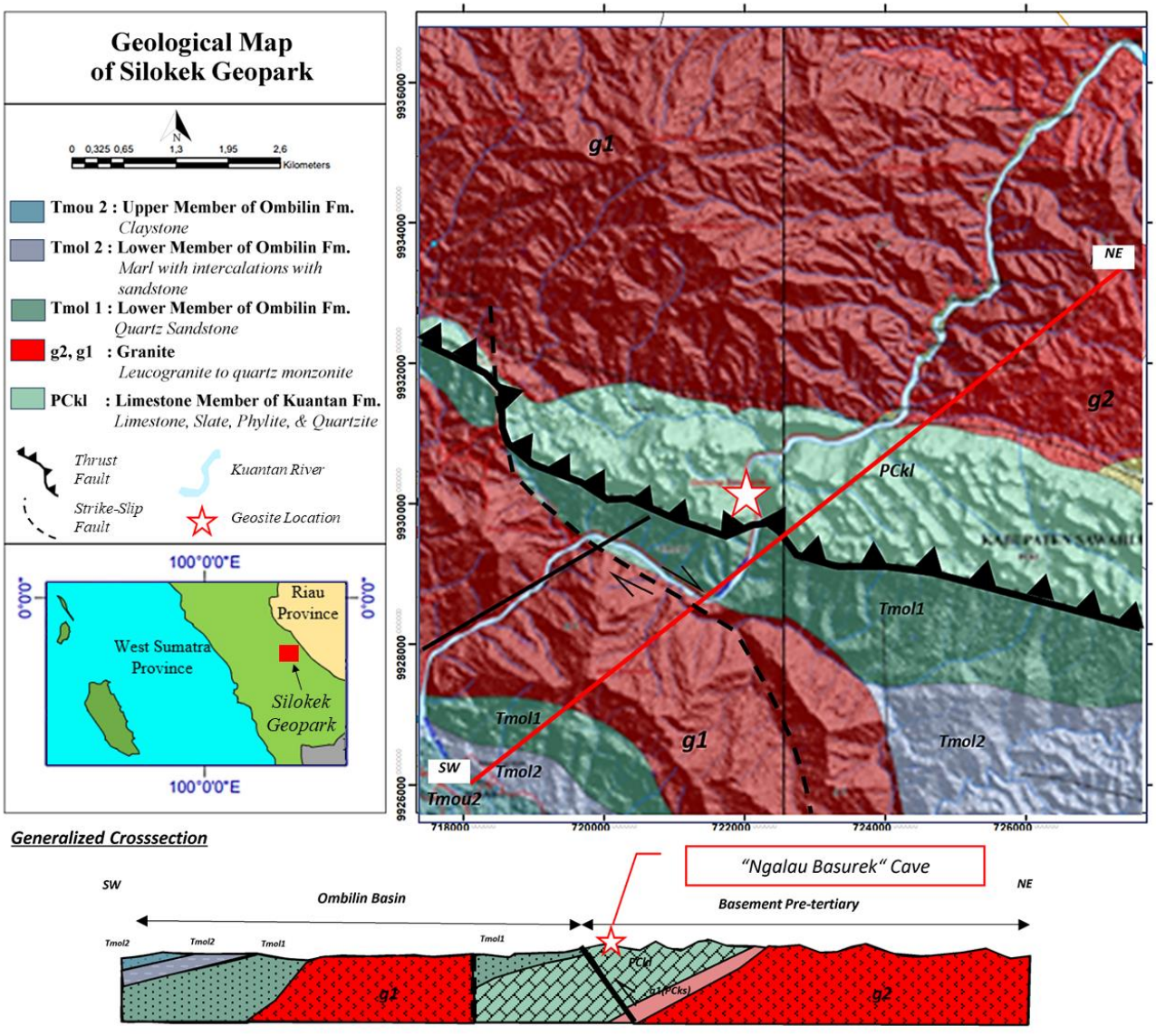


**Figure 1.** A Simplified Geological Map of Silokek Geopark near “Ngalau Basurek” Cave Area.

Ngalau Basurek Cave, the highest-rating geosite (Ummah & Rifai, 2020) is a karst/limestone rock cave made up of calcium carbonate ($CaCO_3$), as illustrated in Figure 2, and is very reactive to solutions of acidic compounds found in water ($CO_2$) that form cavities (Haryono *et al.,* 2022). From the historical point of view, this cave is called "Ngalau Basurek" because the outer wall of the cave bears an inscription believed to have been written in the Dutch era from May to October 1927. This inscription was written before the construction of the S.S. (Staatsspoorwegen) or the Railway Railroad Project Country. The State Railways Company (Staatsspoorwegen) is a railroad company in the Dutch East Indies (Fikri *et al.,* 2023). The Dutch East Indian government owns this company, which was nationalised by the Indonesian government and changed its name to PT Kereta Api Indonesia (Nugraha & Soekarno, 2013).

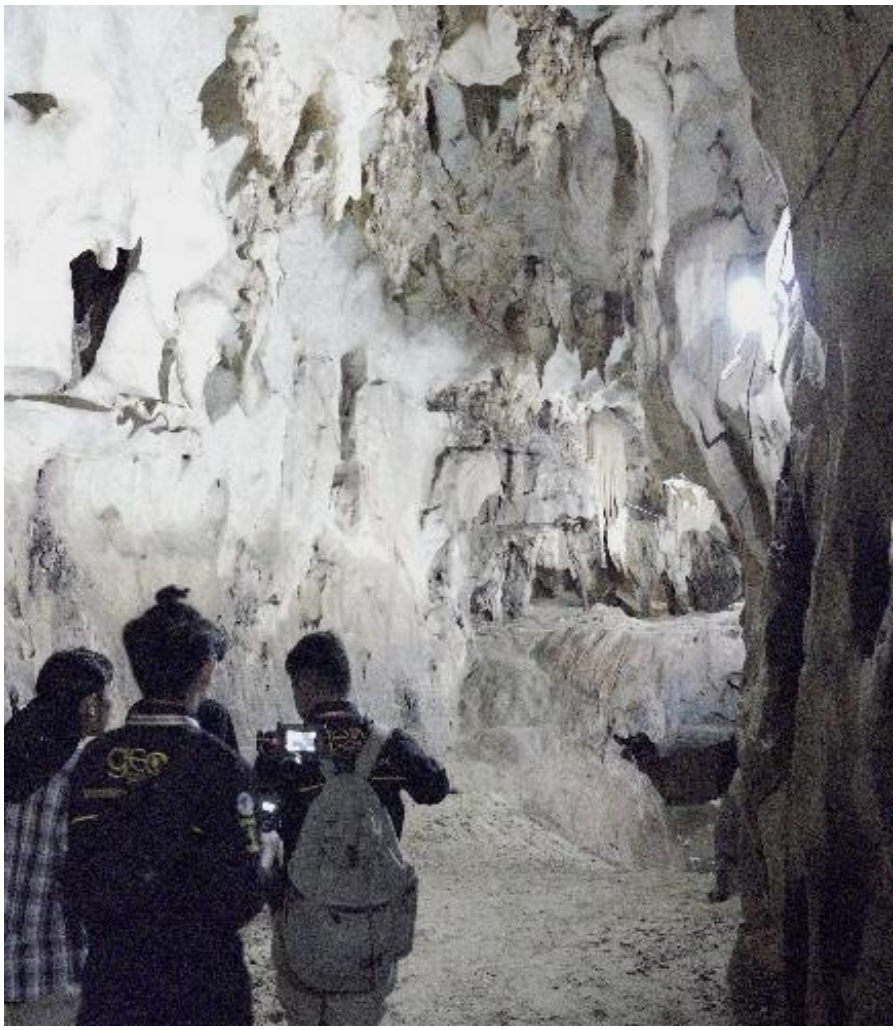

**Figure 2.** The appearance of the Ngalau Basurek cave, which has been facilitated by lighting, shows stalactite ornaments.

The relationship between the morphometry of the cave and the geomorphological patterns on the surrounding surface has not been covered by previous researchers. Consequently, this study aims to describe the patterns that emerge from these two perspectives. Semi-detailed mapping of the Ngalau Basurek Cave and karst-formed undulating hill morphologies on the surface is discussed to do this.

## 3. Research Methods

The methodologies used in this study were divided into two groups: field surveys and studio laboratories. Semi-detailed mapping of the cave floor and roof was carried out using the “compass and step method”, which was modified by adding a Leica Disto D510 Laser Distometer and a geological compass to get a better accuracy of tunnel-like cave convergence measurements (Simeoni & Zanei, 2009). Then, all trends were compared based on the general patterns observed in the cave and the surface terrain, as illustrated in Figure 3.

The semi-detailed mapping can be illustrated in Figure 3, which started with measuring the precise position using a GPS geodetic total station at station NB-1, the first reference point at the main

entrance of the Ngalau Basurek cave with UTM WGS 1984 47S zone coordinate system, then proceeded with determining the next observation station (NB-i) where the distometer will be placed and measuring the distance (d), the slope angle (αi), and the azimuth trevase (Azimuth Pn), so that the position of NB-i (X, Y, Zcorr) can be corrected using the "distometers tripod" height (hdisto) and simple trigonometric relationships using Equations (1), (2), and (3).

$$X = X_i + (d \times Sin\,(Azimuth\ P_n)) \quad (1)$$

$$Y = Y_i + (d \times Cos\,(Azimuth\ P_n)) \quad (2)$$

$$Z_{corr} = (Z_i + (Sin\ \alpha_i)) - h_{disto} \quad (3)$$

Where *X, Y,* and $Z_{corr}$ are the position of the observation station using the UTM WGS84 systems 47S zone, while the $X_i, Y_i,$ and $Z_i$ are the position of the previous station, then $d$ is the measured distance of the previous station in meter domain subsequently, the $Azimuth\ P_n$ is the azimuth between observation and previous station in degree domain, next $h_{disto}$ is the height of distometer stand, later $\alpha_i$ is the slope angle of each traverse station in degree domain.

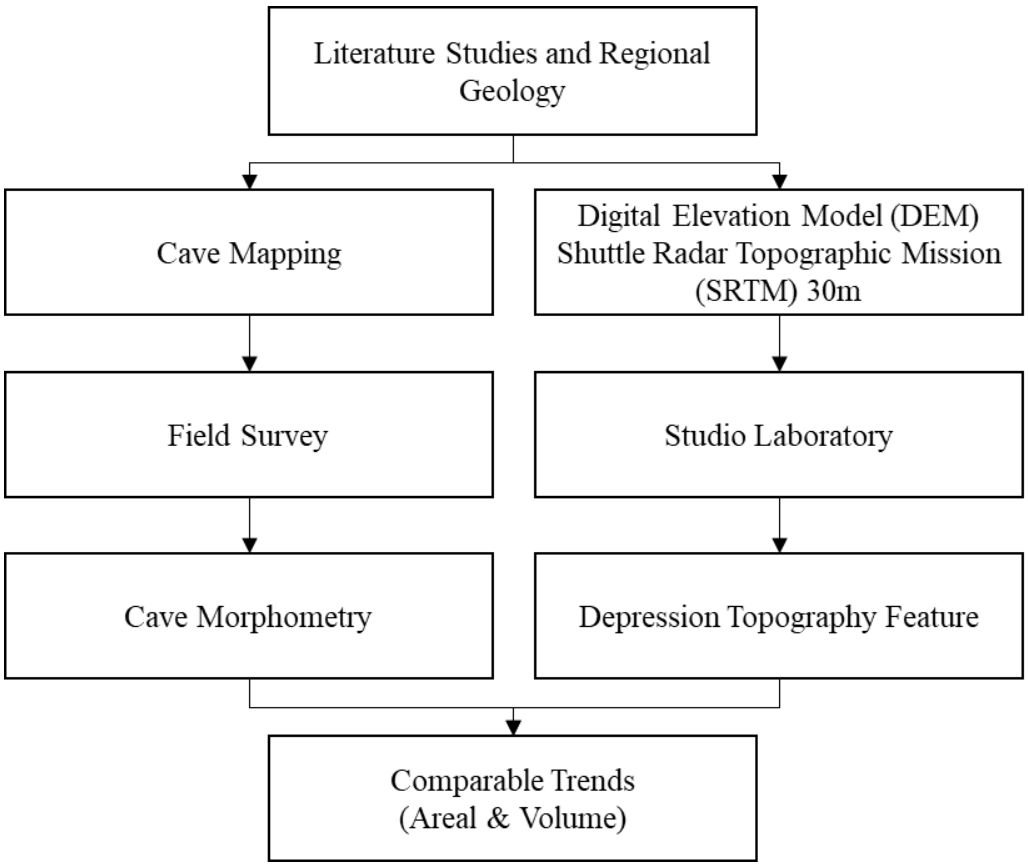


**Figure 3.** The general methodology used to describe the relationship of cave morphometry and surface topography in Silokek Geopark.

Then, the Leica Distometer D510 was used to measure the distance ($l_{\theta n}$) from the NB-I to the attic of the cave. Measurements were conducted to obtain the relative positions from five point clouds at five different angles (0°, 45°, 90°, 135°, and 180°) and then corrected. The analysis started by measuring the azimuth of the profile ($Azimuth\ L_n$) and then corrected by the position of the bases datum reference to get the real coordinates for each point cloud ($X_{\theta n}$, $Y_{\theta n}$, $Z_{\theta n}$) using Equation (4), (5), and (6).

$$X_{\theta_n} = X + \left(Sin\,(Azimuth\ L_n) \times \left(l_{\theta_n} \times Sin\,(\theta_n)\right)\right) \quad (4)$$

$$Y_{\theta_n} = Y + \left(Cos\,(Azimuth\ L_n) \times \left(l_{\theta_n} \times Sin\,(\theta_n)\right)\right) \quad (5)$$

$$Z_{\theta_n} = (Z_i + (l_{\theta_n} \times (Sin\ \theta_n)) \quad (6)$$

Where Xθn,, Yθn,, and Zθn are the position of the point cloud corrected for each angle station using the UTM WGS84 systems 47S zone as summarised in Table 1 and Table 2, while Azimuth Ln is the azimuth of profile section in degree domain, then θn is the angle of distometer (0º, 45º, 90º, 135º, 180º), and lastly, lθn is the distance from the base station to the attic cave (point cloud) measured by distometer.

Using this method, the positions of 78 points on the cave attic were obtained from 15 observation stations, including the cave width (WC) and height (HC), as presented in Tables 3, 4, and 5. Potential hazards from underground river water floods at station NB-15 limited the data. A 3D model of the attic and floor of the Ngalau Basurek Cave was built using a Sequential Gaussian Simulation model from these 78 point clouds using ArcGIS 3Dsoft software for a chaotic pattern to obtain the stalactite and stalagmite features that are more likely to be presented. The direction pattern of the cave morphometry was then obtained from this 3D model (Widyastuti *et al.,* 2023). The Topography Depression Feature Method uses a Digital Elevation Model Shuttle Radar Topography Mission (DEM SRTM) to obtain contour map patterns. The patterns are divided into two main groups, positive and negative, based on the surface undulation terrain and topography, and their pattern is distinguished by the widest regular isolated contour interval (a 10 m contour interval is used in this method). The ArcMap tools from ArcGIS were used to obtain the width, length, and direction of the pattern groups using polygon delineation tools.

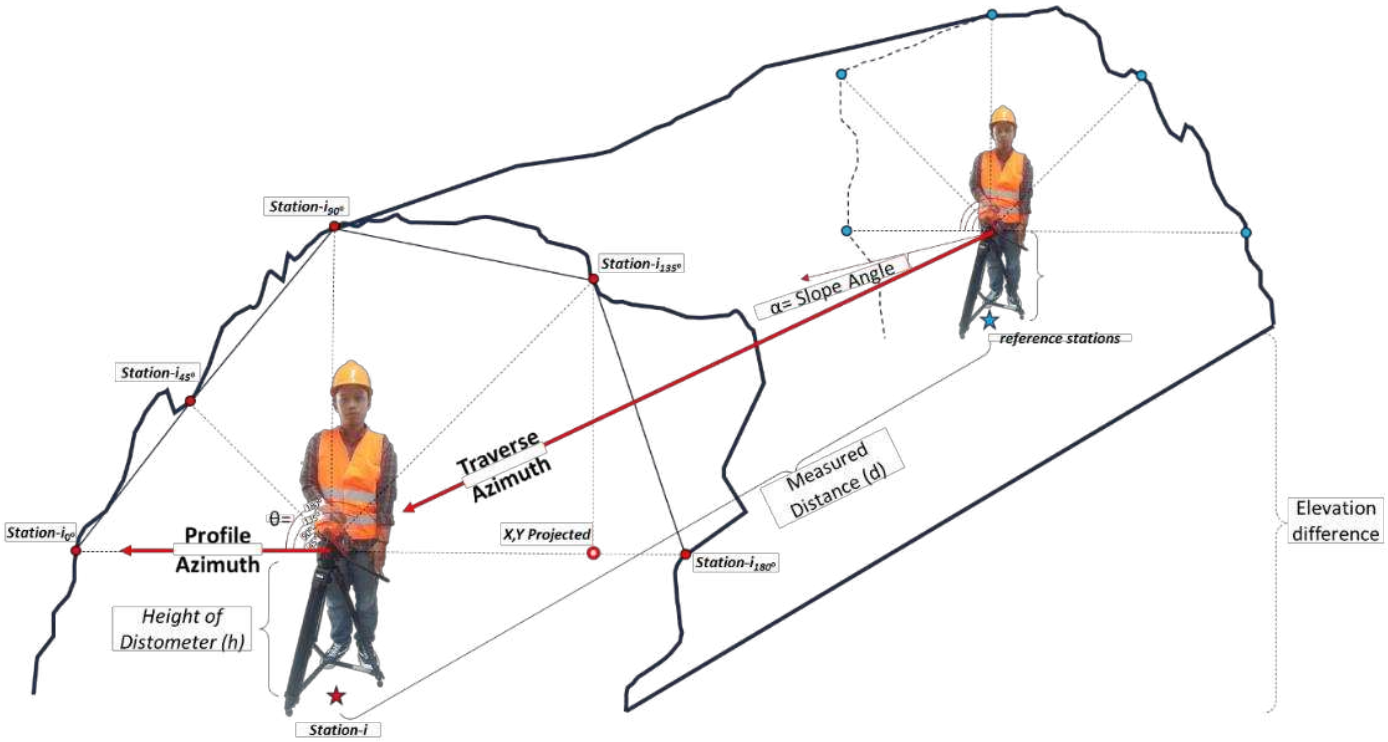


**Figure 4.** Geological Compass, Leica Distometer D510, and Tripod as primary tools were used to get a relative height of the cave's attic, which was then transformed into a corrected position using ArcGIS 3Dsoft software.

**Table 1.** The geometric measurements result from the traverse at each observation station.

| Station | Traverse Azimuth<br>*Azi*<br>[N … °E] | Measured Distance<br>*d*<br>*[m]* | Slope Angle<br>*α*<br>*[°]* | Height of Distometer<br>*h*<br>*[m]* | Profile Direction Azimuth<br>$Azi_x$<br>*[N … °E]* | Wide of Cave<br>$l_{0°} + l_{180°}$<br>*Wc*<br>*[m]* | Height of Cave<br>$l_{90°} + h$<br>*Hc*<br>*[m]* |
|---|---|---|---|---|---|---|---|
| NB01 | 244 | 19.1 | - | 1 | - | - | - |
| NB02 | 244 | 10 | -5 | 1 | 180 | 17.05 | 7.9 |
| NB03 | 300 | 10 | 0 | 1 | 185 | 7.8 | 3.4 |
| NB04 | 304 | 10 | 0 | 1 | 228 | 5.39 | 2.94 |
| NB05 | 315 | 10 | -2.35 | 1 | 221 | 8.7 | 5.5 |
| NB06 | 318 | 10 | 0 | 1 | 254 | 13.01 | 10.14 |
| NB07 | 10 | 10 | 7.1 | 1 | 266 | 6.74 | 4.97 |
| NB08 | 13 | 7.1 | 0 | 1 | 249 | 9.3 | 2.4 |
| NB09 | 17 | 15 | -12.2 | 1 | 210 | 14.47 | 3.34 |
| NB10 | 255 | 17 | 0 | 1 | 197 | 7.5 | 8.63 |
| NB11 | 302 | 15 | 0 | 1 | 223 | 9.51 | 6.82 |
| NB12 | 304 | 15 | 0 | 1 | 212 | 6.2 | 8.15 |
| NB13 | 304 | 12 | 0 | 1 | 230 | 3.45 | 2.32 |
| NB14 | 320 | 8 | 0 | 1 | 223 | 10.6 | 5 |

**Table 2.** The corrected geometric position of each observation station (NB01: Datum Reference).

| Station | Position [ UTM WGS 84 47S] | | | |
|---|---|---|---|---|
| | $X=Xi+(d*Sin\ (Azi))$ X [m] | $Y=Yi+(d*Cos\ (Azi))$ Y [m] | $Z=Z_i+(Sin\ \alpha_i)$ Z [m] | $Z_{corr}=Zi-h$ $Z_{corr}$ [m] |
| NB01 | 722058.29 | 9930193.01 | 122.00 | 121.00 |
| NB02 | 722049.30 | 9930188.63 | 120.34 | 119.34 |
| NB03 | 722040.64 | 9930193.63 | 120.34 | 119.34 |
| NB04 | 722032.35 | 9930199.22 | 120.34 | 119.34 |
| NB05 | 722025.28 | 9930206.29 | 119.93 | 118.93 |
| NB06 | 722018.59 | 9930213.72 | 119.93 | 118.93 |
| NB07 | 722020.33 | 9930223.57 | 121.16 | 120.16 |
| NB08 | 722021.92 | 9930230.49 | 121.16 | 120.16 |
| NB09 | 722026.31 | 9930244.83 | 119.66 | 118.66 |
| NB10 | 722009.89 | 9930240.43 | 119.66 | 118.66 |
| NB11 | 721997.17 | 9930248.38 | 119.66 | 118.66 |
| NB12 | 721984.73 | 9930256.77 | 119.66 | 118.66 |
| NB13 | 721974.78 | 9930263.48 | 119.66 | 118.66 |
| NB14 | 721969.64 | 9930269.61 | 119.66 | 118.66 |

**Table 3.** The position of a measurement point cloud at θ= 0º and θ= 45º for each observation station.

| Station | θ = 0º | | | | θ = 45º | | | |
|---|---|---|---|---|---|---|---|---|
| | $l_{0º}$ | $l_{0º}$ Position | | | $l_{45º}$ | $l_{45º}$ Position | | |
| | | $X_{0º}$ | $Y_{0º}$ | $Z_{corr\ 0º}$ | | $X_{45º}$ | $Y_{45º}$ | $Z_{corr\ 45º}$ |
| NB01 | - | - | - | - | - | - | - | - |
| NB02 | 11.20 | 722049.30 | 9930177.43 | 119.34 | 26.13 | 722049.30 | 9930170.15 | 138.81 |
| NB03 | 4.70 | 722040.23 | 9930188.94 | 119.34 | 5.90 | 722040.28 | 9930189.47 | 124.51 |
| NB04 | 1.62 | 722031.15 | 9930198.13 | 119.34 | 2.68 | 722030.94 | 9930197.95 | 122.23 |
| NB05 | 3.50 | 722022.98 | 9930203.65 | 118.93 | 8.50 | 722021.34 | 9930201.75 | 125.94 |
| NB06 | 4.10 | 722014.65 | 9930212.59 | 118.93 | 6.40 | 722014.24 | 9930212.47 | 124.45 |
| NB07 | 3.60 | 722016.73 | 9930223.32 | 120.16 | 5.20 | 722016.66 | 9930223.31 | 124.84 |
| NB08 | 4.64 | 722017.59 | 9930228.82 | 120.16 | 6.32 | 722017.75 | 9930228.89 | 125.63 |
| NB09 | 1.41 | 722025.60 | 9930243.61 | 118.66 | 1.70 | 722025.71 | 9930243.79 | 120.86 |
| NB10 | 3.25 | 722008.94 | 9930237.32 | 118.66 | 5.10 | 722008.83 | 9930236.98 | 123.27 |
| NB11 | 6.44 | 721992.77 | 9930243.67 | 118.66 | 4.41 | 721995.04 | 9930246.10 | 122.78 |
| NB12 | 4.02 | 721982.60 | 9930253.36 | 118.66 | 4.71 | 721982.97 | 9930253.94 | 122.99 |
| NB13 | 2.65 | 721972.75 | 9930261.78 | 118.66 | 2.39 | 721973.49 | 9930262.39 | 121.35 |
| NB14 | 6.30 | 721965.34 | 9930265.00 | 118.66 | 5.97 | 721966.76 | 9930266.52 | 123.88 |

**Table 4.** The position of a measurement point cloud at θ= 90º and θ= 135º for each observation station.

| Station | θ = 90º | | | | θ = 135º | | | |
|---|---|---|---|---|---|---|---|---|
| | $l_{90º}$ | $l_{90º}$ Position | | | $l_{45º}$ | $l_{135º}$ Position | | |
| | | $X_{90º}$ | $Y_{90º}$ | $Z_{corr\ 90º}$ | | $X_{135º}$ | $Y_{135º}$ | $Z_{corr\ 135º}$ |
| NB01 | - | - | - | - | - | - | - | - |
| NB02 | 6.90 | 722049.30 | 9845293.62 | 127.24 | 4.88 | 722049.30 | 9930192.08 | 123.79 |
| NB03 | 2.40 | 722040.64 | 9845298.62 | 122.74 | 1.42 | 722040.73 | 9930194.63 | 121.34 |
| NB04 | 1.94 | 722032.35 | 9845304.21 | 122.28 | 2.27 | 722033.54 | 9930200.29 | 121.94 |
| NB05 | 4.50 | 722025.28 | 9845311.28 | 124.43 | 4.20 | 722027.23 | 9930208.53 | 122.90 |
| NB06 | 9.14 | 722018.59 | 9845318.71 | 129.07 | 5.32 | 722022.21 | 9930214.76 | 123.69 |
| NB07 | 3.97 | 722020.33 | 9845328.56 | 125.13 | 2.84 | 722022.33 | 9930223.71 | 123.17 |
| NB08 | 1.40 | 722021.92 | 9845335.48 | 122.56 | 1.37 | 722022.83 | 9930230.83 | 122.13 |
| NB09 | 2.34 | 722026.31 | 9845349.82 | 122.00 | 8.75 | 722029.40 | 9930250.19 | 125.85 |
| NB10 | 7.63 | 722009.89 | 9845345.42 | 127.29 | 6.81 | 722011.30 | 9930245.04 | 124.48 |
| NB11 | 5.82 | 721997.17 | 9845353.37 | 125.48 | 4.41 | 721999.29 | 9930250.66 | 122.78 |
| NB12 | 7.15 | 721984.73 | 9845361.76 | 126.81 | 5.56 | 721986.81 | 9930260.10 | 123.59 |
| NB13 | 1.32 | 721974.78 | 9845368.47 | 120.98 | 0.77 | 721975.20 | 9930263.83 | 120.21 |
| NB14 | 4.00 | 721969.64 | 9845374.60 | 123.66 | 3.90 | 721971.52 | 9930271.62 | 122.42 |

**Table 5.** The position of a measurement point cloud at θ= 180º for each observation station.

| Station | θ = 180º | | | |
|---|---|---|---|---|
| | $l_{180º}$ | $l_{180º}$ Position | | |
| | | X 180º | Y 180º | $Z_{corr\ 180º}$ |
| NB01 | - | - | - | - |
| NB02 | 5.85 | 722049.30 | 9930194.48 | 119.34 |
| NB03 | 3.10 | 722040.91 | 9930196.71 | 119.34 |
| NB04 | 3.77 | 722035.15 | 9930201.74 | 119.34 |
| NB05 | 5.20 | 722028.69 | 9930210.21 | 118.93 |
| NB06 | 7.91 | 722026.19 | 9930215.90 | 118.93 |
| NB07 | 3.14 | 722023.46 | 9930223.79 | 120.16 |
| NB08 | 9.43 | 722030.73 | 9930233.87 | 120.16 |
| NB09 | 13.06 | 722032.84 | 9930256.14 | 118.66 |
| NB10 | 4.25 | 722011.13 | 9930244.50 | 118.66 |
| NB11 | 3.07 | 721999.26 | 9930250.63 | 118.66 |
| NB12 | 2.18 | 721985.89 | 9930258.62 | 118.66 |
| NB13 | 0.80 | 721975.40 | 9930263.99 | 118.66 |
| NB14 | 4.30 | 721972.57 | 9930272.75 | 118.66 |

## 4. Results and Discussion

### 4.1. Ngalau Basurek Cave's Morphometry

Ngalau Basurek Cave has several kart ornaments such as stalactites, stalagmites, flowstones, gour-dams, and underground rivers. Generally, The Ngalau Basurek Cave has a length of 140 m and is categorised as a dry zone. The remainder is more than one meter deep in the underground river and is categorised as a wet zone. From these 15 stations, the total area and volume of Ngalau Basurek Cave were at least 760.08 $m^2$ of area and 4111.63 $m^3$, respectively, as presented by the 3D underground surface model in Figure 4. Generally, the 3D model showed an N315 °E trend; however, an anomalous trend exists near NB-05 Station until NB-10 Station. The deflection trend of the cave is presented along with topographical changes on the cave floor and the existence of an underground river. Residents used a combination of these two features to build a dam. Because of this, the dry zone is divided into three main chambers that are classified as safe for tourism sites: first, an entrance chamber (127.53 $m^2$) near the NB-02 to NB-03 stations; second, a water dam chamber (262.84 $m^2$) near the NB-04 to NB-09 stations; and third, a flooding chamber (369.71 $m^2$) near the NB-10 to NB-14 stations, presented by the 2D section trough traverse line in Figure 5.

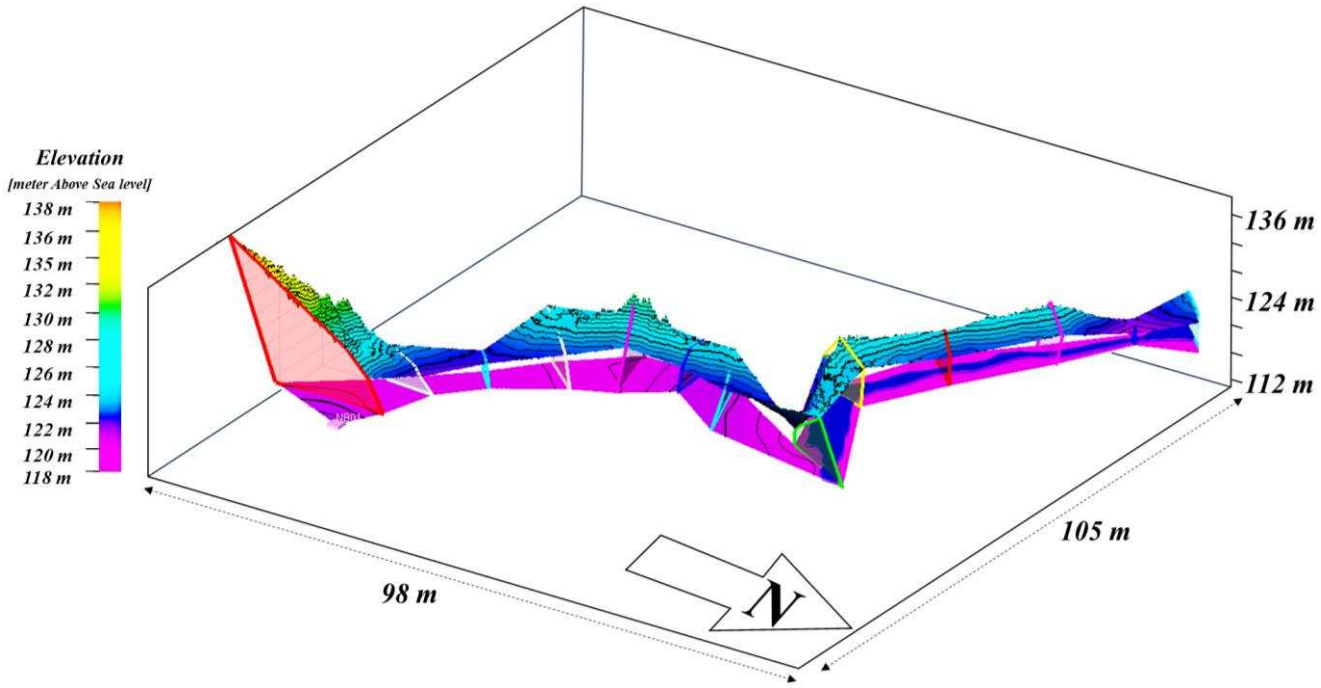


**Figure 5.** 3D model of the attic and floor of Ngalau Basurek and height probability of the attic to the cave floor.

The height between the attics and the floor cave calculated from the 3D model showed varying results; however, the trend direction was still almost the same. In addition, the angle of the cave attic's surface and direction were fairly sharp, with the dominant direction being N 45 °E, as illustrated in Figure 6. In general, Ngalau Basurek Cave has an average height of 5.4 m. However, this varies widely depending on the chamber zone, with the tallest cave chamber being at the entrance chamber (14.97 m), followed by the water dam chamber (10.68 m), and finally (the flooding chamber (9.12 m), as shown in Figure 7.

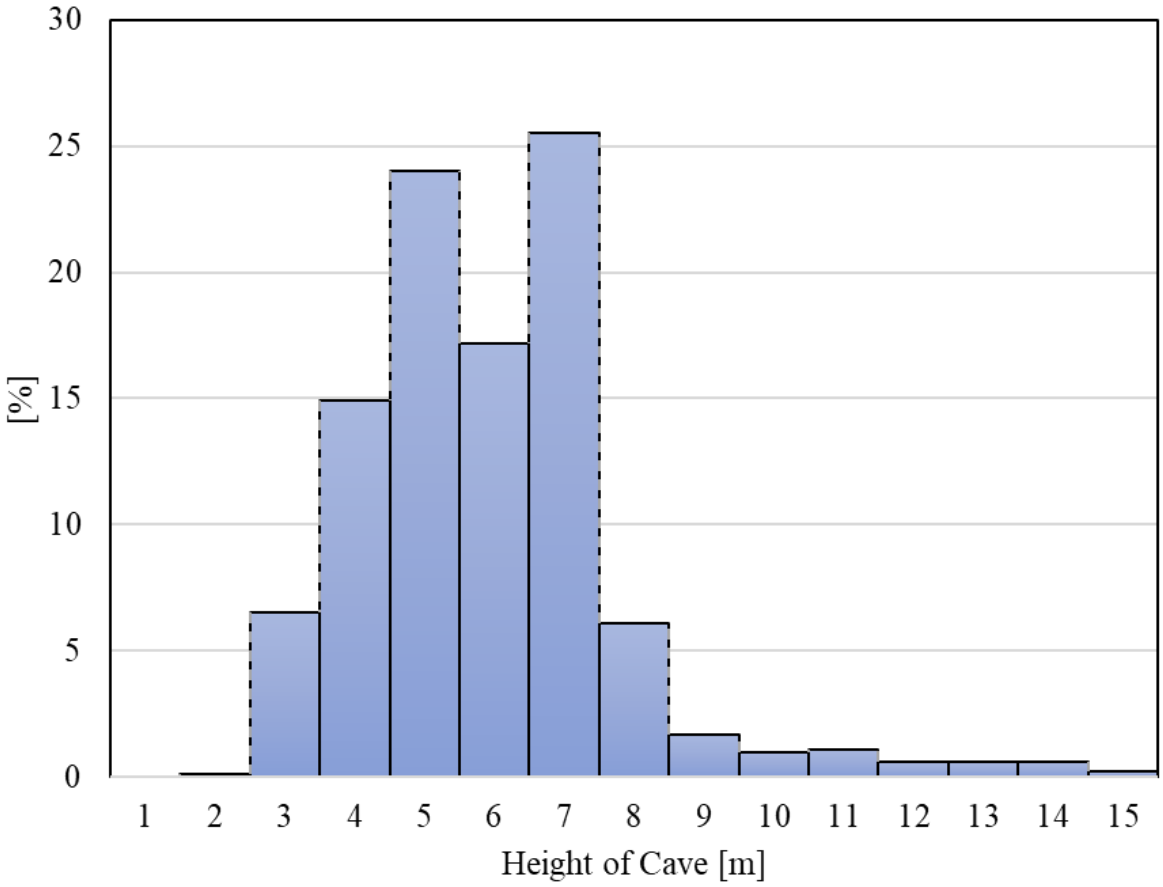


**Figure 6.** The histogram of The Ngalau Basurek cave's shows a bimodal distribution of height.

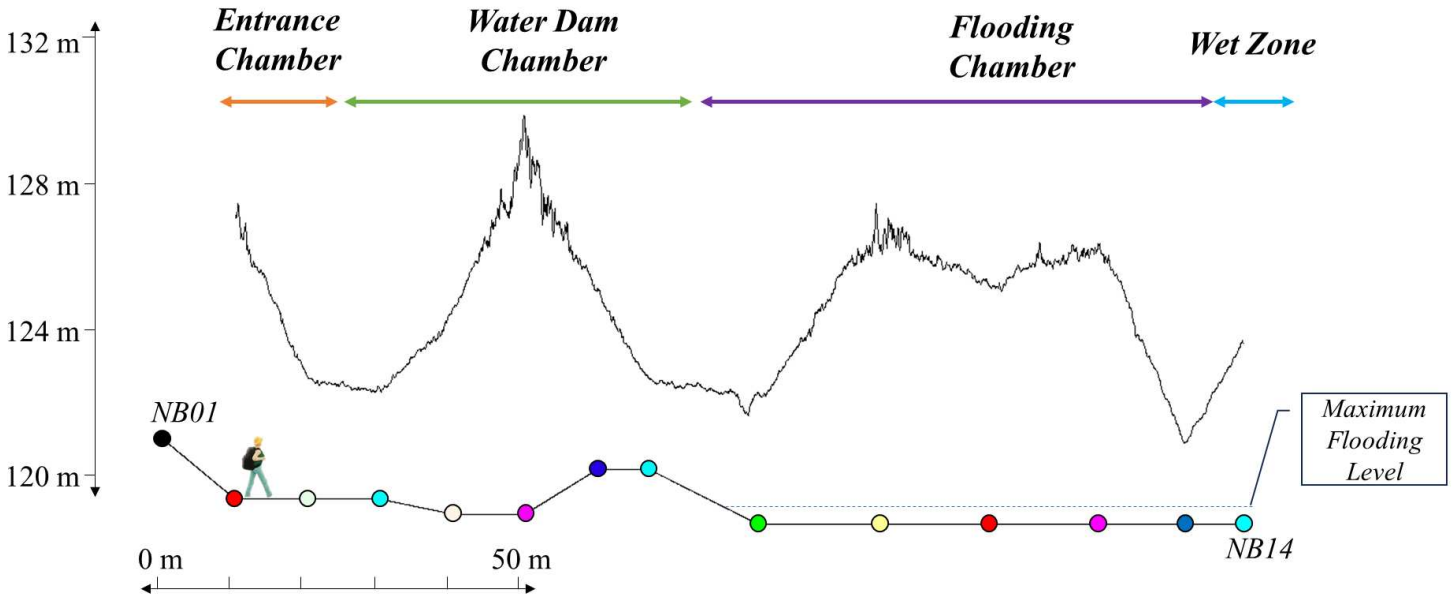


**Figure 7.** Crosssection of the floor and attic of the cave along the traverse station with a 1:5 vertical-horizontal exaggeration ratio; however, the blue-dash line represents the water column of the underground river.

**Table 6.** The average of the Ngalau Basurek Cave morphometry for each interpreted zone.

| No | Zone | Azimuth of Major [N … ⁰ E] | Length Major [ m ] | Length Minor [ m ] | Ratio [ m/m ] | Average Angle of Attics [Degree] | Average Thickness [ m ] |
|---|---|---|---|---|---|---|---|
| 1 | The Entrance Chamber | 309 | 21.5 | 8.6 | 1 : 2.5 | 46.5 | 6.3 |
| 2 | The Water Dam Chamber | 351 | 45.7 | 16.5 | 1 : 2.7 | 37.8 | 4.9 |
| 3 | The Flooding Chamber | 298 | 57.2 | 22.0 | 1 : 2.6 | 39.5 | 5.4 |

From the angle direction aspect criteria in Table 6, the NNE trend dominated the Flooding Chambers. However, some anomalies were observed in the Water Dam Chamber. These abnormalities were followed by changes in cave azimuth, land subsidence on the cave floor, and the disappearance of underground rivers. So, the Water dam Chamber and The Entrance Chamber are integrated into new criteria and produce a 1 to 1.8 length ratio on minor and major with N 298º E anisotropic trend azimuth meanwhile, the flooding chamber has an azimuth trend of N 327º E.

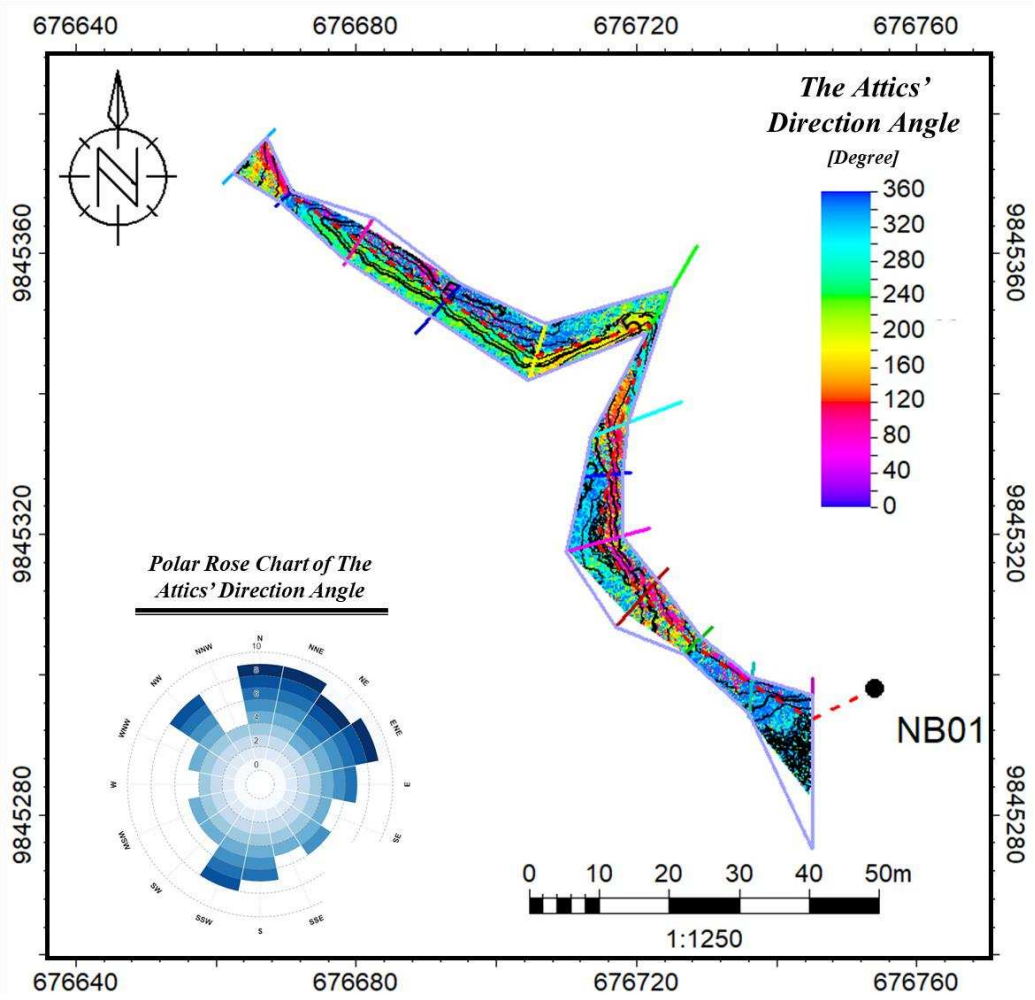


**Figure 8.** The attics' direction angle of the Ngalau Basurek Cave shows the majority trend toward the NNE dominant.

## 4.2. Discussion

Karst landscape is a completely unique type of natural terrain, distinguished by its intricate combination of surface and underground features. Unlike other landscapes that only manifest on the Earth's surface, the karst landscape comprises both terraneous and subterranean components, including caves, channel networks, and cavities. These two parts of the karst landscape are interconnected in numerous ways to form an integrated unit (Andreychouk, 2016). The process of karstification, which involves the dissolution of soluble rocks such as limestone, dolomite, and gypsum, results in a variety of distinctive surface and underground karst features (Gregorič, 2021). This unique formation process leads to landscapes characterised by sinkholes, vertical shafts, disappearing streams, and springs, which are often found alongside vast underground

systems of caves and drainage channels. As depicted in Figure 9, the positive and negative topographical features of the karst area were analysed using the Digital Elevation Model Shuttle Radar Topography Mission (DEM SRTM), as shown in Figure 10. The analysis identified 97 polygons representing positive enclosures with an average area of 0.0333 km² and 67 polygons indicating negative enclosures with an average area of 0.0161 km². These features are a testament to the dynamic processes that shape karst terrain, where erosion and dissolution continually modify the landscape. Rose diagram analysis revealed a similar azimuth trend for each group oriented at 315 °N E, indicating a common directional pattern influenced by the underlying geological structures.

**Figure 9.** The appearance of the karts features shows positive topography (red dash line) and negative topography (blue dash line). The photo was taken from datum point NB-1 toward the Southeast.

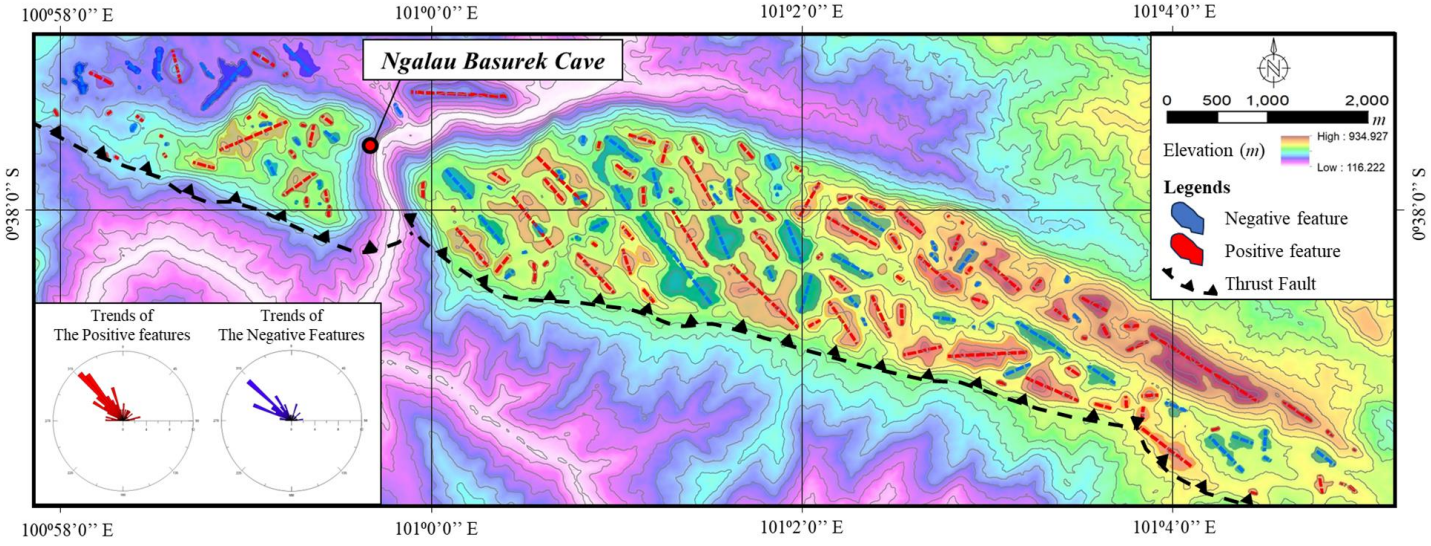


**Figure 10.** The Positive and negative enclosure distribution in Silokek Karts Area indicates the landforms of Karts Tower and Uvala/Doline.

Several nearly perfect ellipsoidal polygons from the negative enclosure group were selected for further analysis. The major and minor length ratios of these polygons were calculated, yielding a value of 1:1.94. Figure 11 illustrates how the dimensions of these negative ellipsoidal shapes vary between the eastern and western faces of the hill, suggesting different erosion rates or structural influences. This interpretation is corroborated by direct observations of karst features such as dolines and uvalas, which are associated with depressions in the landscape. Dolines, also known as sinkholes, form through processes such as the collapse of cave roofs or the dissolution of surface rocks, creating depressions that can vary greatly in size and shape.

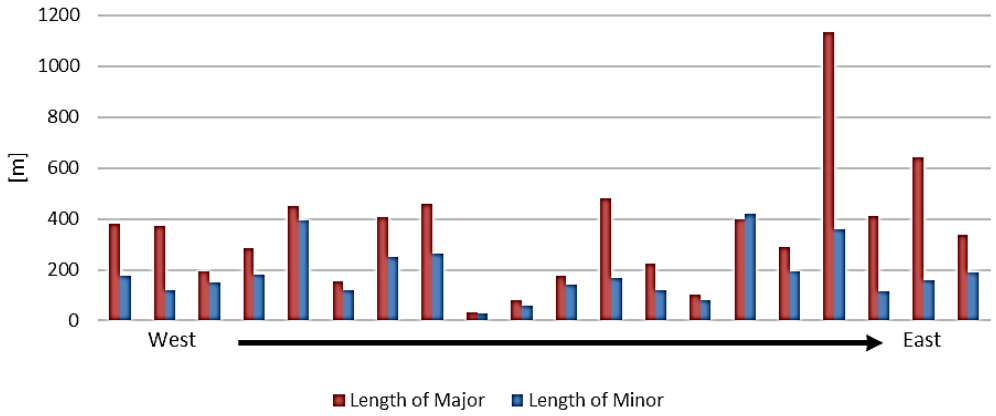


**Figure 11.** Histogram distribution in the length of major and minor for the negative enclosure has a shape almost close to a perfect oval.

Concurrently, the positive features were interpreted as karst cones, as shown in Figure 12. These cones, which are steep conical hills often formed by erosion-resistant remnants of the landscape, stand in stark contrast to the surrounding terrain. The positive and negative features of karst landscapes are integral to understanding the overall geomorphology of these areas. For example, karst cones indicate areas where the surrounding material has been eroded, leaving more resistant rocks behind. This dynamic interplay of erosion and deposition, along with the dissolution processes that characterise karst landscapes, creates highly varied and often spectacular terrain and cave ornaments beneath them.

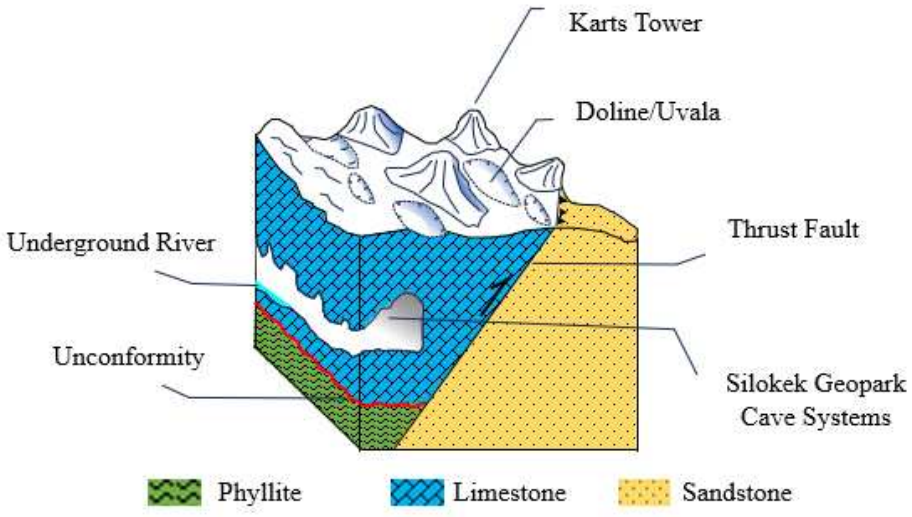


**Figure 12.** 3D illustration of the relationship between surface morphology and cafe morphometry in the Silokek geopark.

In other words, the surface morphology of the Silokek Karst area was intricately shaped by subsurface dissolution processes, exerting varying degrees of influence across the landscape. A notable similarity lies in the northwest trend observed in both cave orientations and depression landscapes, indicating a common geological control. However, a nuanced relationship emerged as the distribution pattern of depressions appeared perpendicular to the angle of the cave roof, revealing a complex interplay between the structural controls and hydrological dynamics. Moreover, a comparison of the dimension ratios between the underground cavern chambers and surface depressions revealed a significant contrast. The higher dimension ratios observed underground suggest a more pronounced impact of dissolution processes on cavern formation, whereas the surface

landforms exhibit lower ratios. This discrepancy underscores the differential influence of dissolution at varying depths with subsurface processes, exerting a more substantial effect than the surface dynamics. This intricate relationship between subsurface dissolution and surface morphology underscores the dynamic nature of karst landscapes, in which geological forces sculpt landscapes over vast timescales.

## 5. Conclusion

The main goal of this study was to determine the relationship between the geomorphology on the surface of the karts area and the morphometry of unmapped caves using a 3D building approach and to produce a simplified model of the physical form of the karts environment and its relation to the enrichment of knowledge in the field of geotourism which places more emphasis on the scientific aspect of geology. 3D cave mapping (surveying and geomodeling) for geotourism enrichment has the potential to be developed in an effort to promote and conserve geosites in geopark areas to provide added scientific value, which is expected to increase economic aspects in the future, thus becoming a sustainable geoscience-tourism program. The semi-detailed morphometric analysis of this geosite revealed a stronger relationship in the general direction of the cave, which is consistent with the direction of the positive and negative features of the surface morphology, which can be classified as doline or uvala and karts tower landforms. However, when considering both the major and minor ratio lengths or dimensions of each landform shape, fascinating discoveries were made, particularly concerning concepts related to spatial and structural aspects. The relationship of ratio measurements of the landform dimensions increased, particularly east of the geopark area, which corresponds to the change in landform direction caused by the thrust fault, which is almost west-east trending. This relationship demonstrates that the kart dissolution process at the development stage of the cave and underground river systems in Silokek Geopark occurred before the uplift; therefore, the cave structure still records the previous palaeomorphology of the carbonate systems. Understanding these processes not only provides insights into the geological evolution of the Silokek Karst area but also has practical implications for land management and environmental conservation in karst regions worldwide. By employing advanced mapping technologies and methodologies, this study provides a comprehensive model of cave morphology that offers insights into cave formation and development. This approach serves as a framework for future research and practical applications in geotourism and geoconservation, ensuring the long-term protection and appreciation of natural and cultural sites. The complexities of this unique landscape allow researchers to gain a deeper understanding of the dynamic interplay between subsurface processes and surface expression, paving the way for informed decision making and sustainable stewardship of karst environments.

**Acknowledgements**

The authors wish to thank the Department of Geography-Social Science Faculty of Universitas Negeri Padang (UNP) and Ranah Minang Silokek Geopark Management Agency for their permission to publish this paper.

**Author Contributions**

**Conceptualisation**: Caesario, D., Khorniawan, W.B.; **methodology**: Susetyo, B. B., Caesario, D.; **investigation**: Sari, W. K., Caesario, D., Ridwan, R.; **writing—original draft preparation**: Caesario, D., Khorniawan, W. B., Sari, W. K.; **writing—review and editing**: Caesario, D., Khorniawan, W. B., Sari, W. K.; **visualization**: Caesario, D., Susetyo, B. B., Ridwan, R. All authors have read and agreed to the published version of the manuscript.

**Conflict of interest**

All authors declare that they have no conflicts of interest.

**Data availability**

Data is available upon Request.

**Funding**

Thanks are given to the Institute for Research and Community Service (LPPM) of Universitas Negeri Padang for Supporting reseach funds

## References

Afrasiabian, A., Sivand, S. M., Dogančić, D., Plantak, L., & Durin, B. (2021). Geological features for geotourism in the zanjan and hamadan area, northern iran. *Sustainability (Switzerland)*, 13(12). doi: 10.3390/su13126587

Andreychouk, V. (2016). The system nature of karst landscape and principles of cave protection resulting from it. *Zeitschrift Für Geomorphologie, Supplementary Issues*, 60(2), 257–291. doi: 10.1127/zfg_suppl/2016/00300

Antić, A., Marković, S. B., Marković, R. S., Cai, B., Nešić, D., Tomić, N., Mihailović, D., Plavšić, S., Radakovic, M. G., Radivojević, A., Sotirovski, D., Ćalić, J., Atanasijević, J., Gavrilov, M. B., Vukojević, D., & Hao, Q. (2022). Towards Sustainable Karst-Based Geotourism of the Mount Kalafat in Southeastern Serbia. *Geoheritage,* 14(1). doi: 10.1007/s12371-022-00651-6

Bahri, S., & Suwijanto. (2014). *Peta Geologi Hasil Interpretasi Citra Inderaan Jauh Lembar Sijunjung Provinsi Sumatera Barat [Map].* Badan Geologi Pusat Survei Geologi Kementerian Energi Dan Sumber Daya Mineral. Retrivied ftom https://geoportal.esdm.go.id/

Chiarini, V. (2022). A Global Perspective on Sustainable Show Cave Tourism. *Geoheritage*, 14(3). doi: 10.1007/s12371-022-00717-5

Fadhly, A., & Hadiyansyah, D. (2020). Studi Morfologi Dan Geologi Kawasan Karst Dalam Pengembangan Konsep Geopark Daerah Silokek, Kabupaten Sijunjung, Sumatera Barat. *Jurnal Sains dan Teknologi: Jurnal Keil-muan dan Aplikasi Teknologi Industri,* 20(2), 228. doi: 10.36275/stsp.v20i2.275

Fikri, A., Isjoni, I., Maulana, Y. S., & Arbain, A. (2023). The Pahlawan Kerja Train Monument Pekanbaru Correlates with Indonesian History Learning Materials In Grade XI In High School. *Yupa: Historical Studies Journal*, 7(1), 73–85. doi: 10.30872/yupa.v7i1.1857

Frey, M., L. (2021). Geotourism—Examining Tools for Sustainable Development. *Geosciences*, 11(30), 1–28. : 10.3390/geosciences11010030

Gregorič, A. C. (2021). Typical Doline and Surface Landforms of Kras (Slovenia): Karst Landscape Features and Possibilities for Their Conservation. *Geoheritage*, 13(2), 26. doi: 10.1007/s12371-021-00544-0

Haryono, E., Reinhart, H., Rabbani, D. I., Putra, R. D., Sukarno, B., Sasongko, M. H. D., Afid, N., Hakim, L., Ristiawan, A. W., & Susanto, A. D. (2022). Study of geotourism development in Batumilmil Karst, Langkat, Sumatera Utara. *IOP Conference Series: Earth and Environmental Science*, 1039(1). doi: 10.1088/1755-1315/1039/1/012056

Hassi, M. F. E. (2022). An Inventory Study of the Geosites in the Area From Susa to Darnah in Al Jabal al Akhdar, Libya: A Proposed Geopark. *Geoheritage*, 14(4). doi: 10.1007/s12371-022-00755-z

Husein, S., Barianto, D. H., Novian, M. I., Putra, A. F., Saputra, R., Rusdiyantara, M. A., & Nugroho, W. (2018). *Perspektif Baru Dalam Evolusi Cekungan Ombilin Sumatera Barat.* Retrivied from https://www.researchgate.net/publication/328703985_Perspektif_Baru_dalam_Evolusi_Cekungan_Ombilin_Sumatera_Barat

Justice, S. (2018). UNESCO Global Geoparks, Geotourism and Communication of the Earth Sciences: A Case Study in the Chablais UNESCO Global Geopark, France. *Geosciences*, 8(5), 149. doi: 10.3390/geosciences8050149

Kirchner, K., & Kubalíková, L. (2014). *Geosite And Geomorphosite Assessment For Geotourism Purpose: A Case Study From The Vizovicka Vrchovina Highland, Eastern Moravia*. Retrivied from https://www.researchgate.net/publication/280095934_GEOSITE_AND_GEOMORPHOSITE_ASSESSMENT_FOR_GEOTOURISM_PURPOSE_A_CASE_STUDY_FROM_THE_VIZOVICKA_VRCHOVINA_HIGHLAND_EASTERN_MORAVIA

Koesoemadinata, R. P. (1981). Stratigraphy and sedimentation: Ombilin Basin, Central Sumatra (West Suma-tra Province). Proc. Indon Petrol. Assoc., 10th Ann. Conv. *Tenth Annual Convention*. doi: 10.29118/IPA.343.217.249

Kubalíková, L. (2013). Geomorphosite assessment for geotourism purposes. *Czech Journal of Tourism*, 2(2), 80–104. doi: 10.2478/cjot-2013-0005

Kusuma, D. W. (2019). Geopark Silokek Sijunjung Menuju UNESCO Global Geopark. *Jurnal Pembangunan Nagari*, 4(1), 17. doi: 10.30559/jpn.v4i1.148

Marjanović, M. (2021). Assessing the Geotourism Potential of the Niš City Area (Southeast Serbia). *Geoheritage*, 13(3). doi: 10.1007/s12371-021-00597-1

Ngwira, P. M. (2019). A Review of Geotourism and Geoparks: Is Africa missing out on this new mechanism for the development of sustainable tourism?. *Geoconservation Research*, 2(1). doi: 10.30486/gcr.2019.666592

Nugraha, A., & Soekarno, S. (2013). The Effect Of Soekarno-Hatta International Airport – Jakarta Railway Train Pro-ject To Pt Kereta Api Indonesia Financial Performance. *The Indonesian Journal of Business Administration*, 2(1), 6–16.

Patzak, M., & Eder, W. (1998). "UNESCO GEOPARK" A new Programme—A new UNESCO label. *Geologica Balcanica,* 28(3–4), 33–35. doi: 10.52321/GeolBalc.28.3-4.33

Pica, A., Lämmle, L., Burnelli, M., Del Monte, M., Donadio, C., Faccini, F., Lazzari, M., Mandarino, A., Melelli, L., Perez Filho, A., Russo, F., Stamatopoulos, L., Stanislao, C., & Brandolini, P. (2024). Urban Geomorphology Methods and Applications as a Guideline for Understanding the City Environment. *Land*, 13(7), 907. doi: 10.3390/land13070907

Sen, S., Migoń, P., Almusabeh, A., & Abouelresh, M. O. (2023). Jabal Al-Qarah, Saudi Arabia—From a Local Tourist Spot and Cultural World Heritage to a Geoheritage Site of Possible Global Relevance. *Geoheritage*, 15(4). doi: 10.1007/s12371-023-00879-w

Silitonga, P. H., & Kastowo. (1995). *[Map] (2nd edition). Pusat Penelitian dan Pengembangan Geologi*. Retrieved from https://geoportal.esdm.go.id/

Simeoni, L., & Zanei, L. (2009). A method for estimating the accuracy of tunnel convergence measurements using tape distometers. *International Journal of Rock Mechanics and Mining Sciences*, 46(4), 796–802. doi: 10.1016/j.ijrmms.2008.11.004

Štrba, Ľ., & Molokáč, M. (2022). Geotourism and Geoparks—Promoting Geoheritage and Geodiversity to People. *World Geomorphological Landscapes, Query*, 437–449. doi: 10.1007/978-3-030-89293-7_22

Ummah, K., & Rifai, H. (2020). Preliminary analysis learning media based on edupark science with scientific methods in the national geopark of Ranah Minang Silokek of Sijunjung. *Journal of Physics: Conference Series*, 1481(1), 012065. doi: 10.1088/1742-6596/1481/1/012065

Widyastuti, R., Saptari, A. Y., Falihah, S. R., Eryan Putri, N. S., & Hernandi, A. (2023). Geometric Model of 3D Cadastre for Strata Title using 2D and 3D Data Integration Approach. *IOP Conference Series: Earth and Environmental Science,* 1276(1), 012007. doi: 10.1088/1755-1315/1276/1/012007